

# An evaluation of potential solar radio emission power threat on GPS and GLONASS performance

Vladislav V. Demyanov · Edward L. Afraimovich · Shuanggen Jin

Received: 8 October 2010 / Accepted: 11 October 2011 / Published online: 1 November 2011  
© Springer-Verlag 2011

**Abstract** The L-band solar radio emission has recently been regarded as a potential threat to stable GPS and GLONASS performance. However, the threat has not been completely investigated or assessed so far. We evaluate in detail the occurrence of GPS/GLONASS signal tracking failures under the direct exposure of wideband solar radio emission. By means of theoretical analysis, we found that the solar radio emission power level of 1,000 sfu (solar flux units) or higher can cause GPS/GLONASS signal tracking failures especially at L2 frequency. In order to prove this evaluation, we investigated GPS/GLONASS signal tracking failures at L1 and L2 frequencies during power solar flares X6.5 (December 6, 2006) and X3.4 (December 13, 2006). Comparing these events with weaker solar flare X17.2 on October 28, 2003, we found that L2 signal tracking failures appeared when the solar radio emission power exceeds 1,000 sfu. Therefore, our theoretical and experimental results confirm the earlier results by other authors.

**Keywords** Solar flares · Solar radio emission · GPS · GLONASS performance

## Introduction

Until recently, the L-band solar radio emission was not considered as a potential threat to the stable performance of satellite radio-navigation systems such as GPS and GLONASS (Chen et al. 2005; Jin et al. 2008). Power threshold of the solar radio emission at the level of 40,000 sfu (solar flux units), which still provided steady performance of GPS, was found by Klobuchar et al. (1999). However, only several solar radio bursts with the power level higher than 40,000 sfu have been observed over the last 40 years (Cerruti et al. 2006; Chen et al. 2005).

According to Carrano et al. (2007), the signal-to-noise ratio decreases by 10–30 dB depending on the angular position of the sun relative to the directional pattern of receiver antenna under the direct influence of the solar radio emission. It causes failure in signal tracking of many visible navigation satellites on the earth's dayside for up to 1 h.

Detailed investigation of solar radio emission interference on the GPS equipment performance indicated that the unsafe threshold of the solar radio emission power should be reduced to 4,000–12,000 sfu. A specific value of this threshold should be determined according to the type of signal tracking algorithms which are utilized in GPS/GLONASS user equipment.

As it was proven by Afraimovich et al. (2008) and Cerruti et al. (2006), many short-term failures in measurements of radio-navigation parameters were observed in GPS and GPS/GLONASS receivers all over the world during strong solar radio bursts on December 6 and 13, 2006. Some failures in measurements of radio-navigation parameters

---

The article is dedicated to the memory of Prof. E. L. Afraimovich who founded the Irkutsk scientific school for GPS sounding of the ionosphere and effectively worked as a mentor of this school for years.

---

V. V. Demyanov (✉)  
Irkutsk State Railway University, P. Box-102,  
664009 Irkutsk, Russia  
e-mail: sword1971@yandex.ru

E. L. Afraimovich  
Institute of Solar-Terrestrial Physics, The Russian Academy  
of Sciences, The Siberian Branch, Irkutsk, Russia

S. Jin  
Shanghai Astronomical Observatory,  
Chinese Academy of Sciences, Shanghai 200030, China

were recorded even when the solar radio flux power was as much as  $3 \times 10^3$  sfu (Afraimovich et al. 2008).

Nevertheless, a detailed analysis of separate solar radio bursts impact on the GPS/GLONASS user navigation equipment is required in order to estimate an extent of deterioration of the positioning systems on a global scale. Especially, maximum allowable power of the solar radio emission, which provides satisfactory signal-to-noise ratio at the navigation receiver input, is very important. Such research would allow us to reestimate GPS and GLONASS noise immunity and make necessary improvements into navigation receivers development according to the known impact of the solar radio emission. The aim of this research is to evaluate the unsafe threshold of solar radio emission power for GPS/GLONASS receivers on a basis of theoretical and experimental comparative analysis in the potential noise immunity of GLONASS CT(BT) and GPS CA (P(Y)) dual—frequency receivers.

### The solar radio emission power at the GPS/GLONASS receiver antenna output

The steady operation of a GPS/GLONASS receiver under the influence of intensive radio interference depends on the characteristics of radiofrequency (RF) chain of navigation receiver within which the main filtering and amplification of satellite signals take place. The exact measurement of solar radio emission power, which affects the radiofrequency chain input, is therefore very important. This measurement is necessary to design optimal algorithms for primary processing and filtering of radio-navigation parameters in the processor of navigation receiver.

Computing of solar radio emission power at the radiofrequency path input should begin with consideration of the receiver antenna directional pattern. The antenna directive gain (AD) is defined as ratio between the power specified for a real antenna  $P(\theta, \beta)$  and the power specified for a reference isotropic antenna ( $P_0$ ), provided that signal powers at the observation point are equal.

$$D(\theta, \beta) = P(\theta, \beta)/P_0 \quad (1)$$

The symbols  $\theta$  and  $\beta$  are the angles of receiving signal in the azimuth and elevation.

First, we should set the characteristics of directional properties of a real receiving antenna. The characteristics we utilized—are that the receiving antenna power gain  $G(\beta)$  relative to the ideal isotropic antenna (Table 1, column 2) and the antenna directive gain— $D(\theta, \beta)$  (Table 1, column 3)—were computed as follows

$$G(\beta) = 10 \cdot \lg(D(\theta, \beta)) \quad (2)$$

**Table 1** Directive characteristics of a navigation receiver antenna (Kaplan 1996)

Elevation angle of signal reception, $\beta^\circ$	$G(\beta)$ in (dB)	$D(\theta, \beta) = P(\theta, \beta)/P_0$
$0 < \beta < 5$	$-7.5 \leq G(\beta) \leq -5$	$0.1775 \leq D(\theta, \beta) \leq 0.316$
$5 < \beta < 15$	$-4.5 \leq G(\beta)$	$0.354 \leq D(\theta, \beta)$
$\beta > 15$	$-2 \leq G(\beta)$	$0.63 \leq D(\theta, \beta)$

**Table 2** Antenna effective area

$\beta^\circ$	$A_e(\beta)$ in (m <sup>2</sup> )	
	$\lambda = 0.190$ in (m) (L1)	$\lambda = 0.244$ in (m) (L2)
$0^\circ < \beta < 5^\circ$	$5.099 \times 10^{-4} \leq A_e(\beta) \leq 9.077 \times 10^{-4}$	$8.409 \times 10^{-4} \leq A_e(\beta) \leq 1.497 \times 10^{-3}$
$5^\circ < \beta < 15^\circ$	$1.01 \times 10^{-3} \leq A_e(\beta)$	$1.677 \times 10^{-3} \leq A_e(\beta)$
$\beta > 15^\circ$	$1.809 \times 10^{-3} \leq A_e(\beta)$	$2.984 \times 10^{-3} \leq A_e(\beta)$

Another property of the receiving antenna to be considered for performing calculations is the antenna effective area. AD values are related to the antenna effective area by

$$D(\theta, \beta) = 4\pi \cdot A_e(\beta)/\lambda^2 \quad (3)$$

where  $\lambda$  is the received signal wavelength and  $A_e$  is the antenna effective area.

Equation (3) implies that the real receiving antenna has AD in the azimuthal plane equal to that of the standard isotropic antenna, i.e. the value  $D(\theta, \beta)$  does not depend on the azimuth of the received signal  $\theta$ . Its elevation angle dependence  $\beta$  has already taken into account in Table 1.

Thus, we can calculate the magnitudes of effective area of the real receiver antenna at two operating frequencies of GPS/GLONASS and different elevation angles. Table 2 contains calculation results for GPS operating frequencies. In our further consideration, we assume that the  $A_e$  values for GLONASS receivers are close to GPS ones.

After determining the main characteristics of the receiving antenna, we can compute the power of the solar radio emission at the receiving antenna output. In order to do this, specifications and assumption are as follows:

- Solar radio emission flux with the power of 1 sfu is equal to the power spectral density corresponding to the interval of 1 Hz of this flux power spectrum passing through the area of 1 m<sup>2</sup>, i.e., 1 sfu =  $10^{-22}$  W m<sup>-2</sup> Hz<sup>-1</sup> (Chen et al. 2005).
- Radio emission of the solar flare relative to an actual satellite signal is considered as the white Gaussian noise. Generally, the noise power  $P_n$  within the given frequency band from  $F_1$  to  $F_2$  is obtained from the noise spectrum  $S(f)$  as follows

$$P_n = \int_{F_1}^{F_2} S(f)df \tag{4}$$

As the solar radio emission intensity  $-N_0$  in the frequency band  $\Delta F_n$  of the satellite signal is constant throughout the band, the radio emission power of a solar flare within the frequency bands of GPS and GLONASS signals can be computed in the similar way, as follows

$$P_n = \Delta F_n \cdot N_0 \tag{5}$$

- c. The solar radio noise has the right-hand elliptical polarization and undergoes attenuation proportional to the polarization mismatch factor of 3.4 dB (at the frequency L1) and 4.4 dB (at the frequency L2) when passing through the antenna (ICD-GPS-200c 1993);
- d. When passing through the atmosphere, the solar radio emission in the GPS (GLONASS) frequency band undergoes the maximum attenuation of  $-2$  dB (ICD-GLONASS 2002; ICD-GPS-200c 1993);

Thus, the power of the solar radio noise  $P_n$  at the receiving antenna output—without considering polarization loss and attenuation in the atmosphere—can be defined as:

$$P_{n,GPS(GLN)} = \Delta F_{n,GPS(GLN)} \cdot k \cdot N_0 \cdot A_e(\beta) \tag{6}$$

where  $k$  is the rate of the solar radio emission flux in terms of sfu and  $N_0 = 10^{-22} \text{ W m}^{-2} \text{ Hz}^{-1}$ .

The value of the solar radio emission power also depends on the sun zenith angle. In Eq. (6), this dependence is expressed in implicit form in terms of  $A_e(\beta)$  calculated from the angle of signal reception (Table 2).

Since it is more convenient to use power units (dBW) for further analysis, the solar radio noise power at the receiving antenna output may be converted to these units as

$$L_{n,GPS(GLN)} = 10 \cdot \lg(P_{n,GPS(GLN)}) \tag{7}$$

If we take into account the polarization loss and attenuation in the atmosphere at the frequencies L1 and L2 (ICD-GPS-200c 1993), we get  $L_{n,GPS(GLN)} = 10 \cdot \lg(P_{n,GPS(GLN)}) - 2 - 3.4$  and  $L_{n,GPS(GLN)} = 10 \cdot \lg(P_{n,GPS(GLN)}) - 2 - 4.4$ , at the frequencies L1 and L2, respectively.

Finally, we can compute the solar radio noise power at the receiving antenna output for solar elevation angles  $>15^\circ$  at the central solar radio emission frequency  $f = 1,415 \text{ MHz}$  (we assumed  $\lambda = 0.212 \text{ m}$ ,  $A_e = 2.253 \times 10^{-3} \text{ m}^2$ , polarization loss =  $-3.4 \text{ dB}$ ) in Table 3.

The front-end passband of the GPS receiver radio path ( $\Delta F_{GPS}$ ) is 3 MHz (Kaplan 1996), while the passband of the GLONASS receiver for the channel of each separate satellite is only 0.5 MHz ( $\Delta F_{GLN}$ ) (Perov and Kharisov 2005). Hence, power of solar radio emission should be

considered only in these narrow frequency bands for GPS and GLONASS correspondently (Table 3).

Here, we should provide some special explanation about the front-end passband of the GPS and GLONASS radio-frequency chain. Generally speaking, the front-end band width should be twice of the chipping rate (1.023 MHz for GPS and 0.511 MHz for GLONASS). However, depending on the navigation receiver specification, the bandwidth can be set significantly larger or lower. Moreover, we should take into account that a navigation receiver utilizes the same RF chain in order to process CA and P(Y) code signals concurrently at the same current frequency (1.5 GHz for GPS and 1.6 GHz for GLONASS). Hence, we can not set RF front-end band width too narrow because it can cause severe phase distortion of the P(Y) or BT signal. On the other hand, we should keep the bandwidth narrow enough for effective suppressing of external radio noise including the solar radio emission. The specific choice depends on the developer of the GPS/GLONASS receiver specification, while it is unknown for us exactly. In order to evaluate the effect of solar radio emission on navigation receivers, we used some averaged values of the RF front-end bandwidth (Table 3).

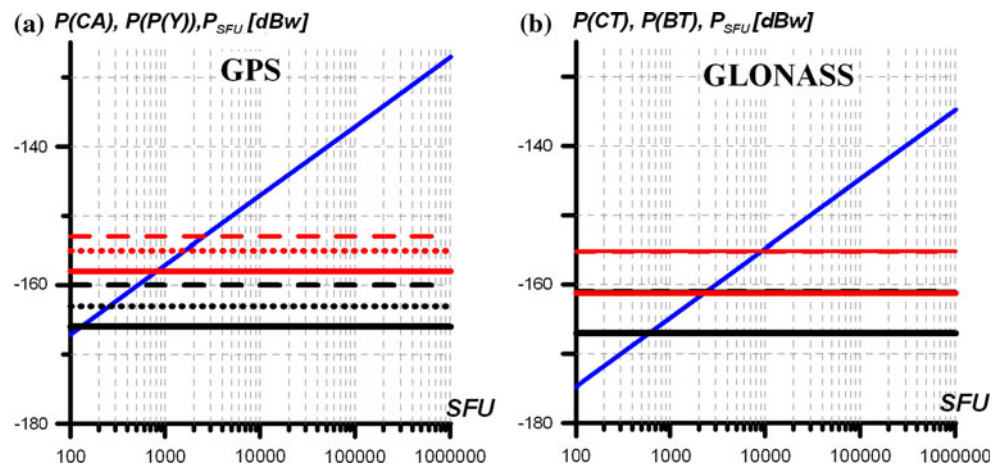
Generally, it is known that GLONASS utilizes FDMA technology to separate the signals of particular GLONASS satellites. It requires to set narrower RF front-end bandwidth in comparing to the GPS one. The main expected consequence is lower integral solar radio noise power at the AD converter input of the navigation receiver.

A comparative plot between powers of GPS and GLONASS received signals and the solar radio emission  $P_{SFU}$  at the output of receiving antenna can be made on the basis of above-mentioned reasons. Figure 1a gives the ratio of powers of the solar radio emission flux and GPS signal components, and Fig. 1b illustrates the case for GLONASS.

The horizontal lines in Fig. 1a indicate levels of minimum (red lines) and maximum (black lines) power of GPS signal components at the receiving antenna output (ICD-GPS-200c 1993). The power levels for the components of coarse acquisition code—CA (P(CA)) and encrypted P(Y)-code (P(P(Y))) at the L1 frequency, and for the P(Y) component at the L2 frequency are presented by dotted lines, dots and solid lines, respectively. The slant line shows power values of the solar radio emission flux  $P_{SFU}$ . Figure 1b has the same notations for the components of the standard precision code (CT) and high-precision code (BT) of GLONASS signals at frequencies L1 and L2 (ICD-GLONASS 2002). As power values of some components are close, these lines partially mix in the diagram. The power values of the solar radio emission flux in terms of sfu are plotted along the horizontal axis with the logarithmic scale.

**Table 3** Rate of the solar radio emission flux

$L_n$ (dBW)	Rate of the solar radio emission flux ( $k$ ), sfu					
	1	$10^2$	$10^3$	$10^4$	$10^5$	$10^6$
$L_{n,GPS}$ (dBW) ( $\Delta F_{GPS} = 3$ MHz)	-187.1	-167.1	-157.1	-147.1	-137.1	-127.1
$L_{n,GLN}$ (dBW) ( $\Delta F_{GLN} = 0.5$ MHz)	-194.8	-174.8	-164.8	-154.8	-144.8	-134.8

**Fig. 1** Power level of the solar radio emission at the receiving antenna output

It is obvious from Fig. 1 that for a solar radio noise within  $10^2$ – $10^4$ , the power of the solar radio noise is compared with power of the satellite signal at the receiving antenna output and exceeds it. When the solar radio emission flux is  $10^6$  sfu, the level of the solar radio noise exceeds the signal by 26–39 dB at the GPS receiving antenna output and by 20–32 dB at the GLONASS receiving antenna output.

### Unsafe threshold of the solar radio emission power for GPS and GLONASS

Based on the above-mentioned estimates, we can determine the unsafe threshold of solar radio noises at which the signal-to-noise ratio at the receiving antenna output is insufficient for stable tracking of satellite signals.

First, we should take into account the fact that a significant gain in the signal-to-noise ratio is observed due to the use of correlation processing of the received signals if the structure of the pseudonoise ranging code is known at the receiving site. This gain (in terms of dBW) can be calculated as follows (Kaplan 1996)

$$SN_{cor} = 10 \cdot \lg \left( \frac{F_{PRN}}{2 \cdot \Delta F_{PD}} \right) \quad (8)$$

where  $F_{PRN}$  is the frequency of elementary pulse in pseudorandom sequences of ranging code:  $F_{PRN} = 1.023 \times 10^6$  MHz for the CA code and  $10.23 \times 10^6$  MHz for the P(Y) code of GPS, or  $0.511 \times 10^6$  MHz for the CT code and

$5.11 \times 10^6$  MHz for the BT code of GLONASS, respectively;  $\Delta F_{PD}$  is the predetector passband that is found from the lowest modulation frequency of the satellite signal by the service information data (50 Hz) (Kaplan 1996; Perov and Kharisov 2005).

Since the CA (CT) code structure is always known, it is obvious that GPS and GLONASS maximum noise immunity under the influence of a powerful solar radio emission takes place for the CA (CT) code at the main operating frequency L1.

On the other hand, L2 GPS signal is only modulated by the encrypted code. “Semicodeless” or “codeless” processing algorithms are widely used in dual-frequency receivers in order to extract the P(Y) or BT-code signal components at the L2 GPS (GLONASS) frequency. Usage of these algorithms with no sufficient data on the P(Y) or BT-code structure reduces the stability of signal tracking at the L2 frequency under the influence of external radio emission (Skone and de Jong 2001). Significant fading of the signal-to-noise ratio while the encrypted signal is extracting and tracking at the L2 frequency may take place depending on the type of correlation processing algorithm. The level of these losses in the signal-to-noise ratio  $\Delta SN_{cor}$  is within 14–17 dB (if “semicodeless” algorithms are utilized) and 27–30 dB (with the use of “codeless” algorithms) (Chen et al. 2005).

Access to the BT signal component of GLONASS and to the P(Y) code in the GPS system is not for common use, and in our examination, we suppose that the correlation losses of BT signal tracking at L2 GLONASS frequency

are equal to ones of GPS. It is known that integration time periods in phase and code tracking loops of GPS (GLONASS) receivers inside the “integrate and dump” module are approximately the same: 1 ms—in the phase tracking loop and 20 ms—in the code tracking loop. The origin of the distortion of the correlation integral under “semicodeless” or “codeless” processing technique for both GPS and GLONASS is the same. Hence, we suppose that correlation losses  $\Delta SN_{cor}$  should also be approximately the same.

When the satellite signal is locked, the coherent tracking of the carrier frequency phase and code delay of the signal starts. The noise immunity of a navigation receiver is defined by the noise immunity level of the phase lock loop (PLL) of the receiver (Kaplan 1996). That is why the unsafe threshold of solar radio emission causing the satellite signal tracking loss should be determined from the level of minimum acceptable signal-to-noise ratio that provides stable performance of the PLL.

The discrimination characteristics of the phase discriminator has a limited linear section; therefore, severe requirements are imposed on the maximal acceptable carrier phase filtering error  $\sigma_{\phi,max}$ . If the error level is exceeded, phase filtration is divergent and the signal tracking loss is observed. Magnitude of filtering error  $\sigma_{\phi}$  of the carrier phase depends on many factors such as receiver thermal noises, short-term instability of reference generator frequency and phase fluctuation, caused by dynamic impact on the navigation satellite. With all the above consideration, we can determine filtering error magnitude of the carrier phase as follows (Kaplan 1996),

$$\sigma_{\phi} = \sqrt{\sigma_T^2 + \sigma_F^2} + \frac{\sigma_S}{3} \leq \sigma_{\phi,max} \tag{9}$$

where  $\sigma_T$ ,  $\sigma_F$  and  $\sigma_S$  are root-mean-square (rms) errors of the carrier phase filtration (in degrees) caused by thermal noises, short-term instability of the reference generator frequency and dynamic stress of the receiver, respectively.

The magnitudes of separate components of Eq. (9) can be calculated from the following formulae (Kaplan 1996),

$$\sigma_T = \frac{360}{2 \cdot \pi} \sqrt{\frac{\Delta F_{PLL}}{cn_0} \cdot \left[ 1 + \frac{1}{2T_{COR} \cdot cn_0} \right]} \tag{10}$$

where  $\Delta F_{PLL}$  is the noise bandwidth of PLL,  $cn_0$  is the signal-to-noise ratio at the receiver input, expressed by the power ratio determined on the basis of the receiver sensitivity, and  $T_{COR}$  is the predetection integration time. The rms error for the short-term instability of reference generator frequency is

$$\sigma_F = 160 \cdot \frac{\sigma_F(\tau) \cdot F_c}{\Delta F_{PLL}} \tag{11}$$

where  $F_c$  is the satellite signal carrier frequency. The rms error for the dynamic stress of the receiver is

$$\sigma_S = 0.4828 \cdot \frac{dR^3/dt^3}{(\Delta F_{PLL})^3} \tag{12}$$

where  $dR^3/dt^3$  is the maximum dynamic stress of the receiver along the “satellite-receiver” line of sight. Expressions (11) and (12) are written for the third-order loop filter which is typically used for signal phase tracking in navigation receivers.

From Eqs. (9)–(12), we can find an expression that defines the minimal allowable signal-to-noise ratio at the receiver input ( $CN_{thr}$ —in terms of dBW) for the maximum allowable value of the phase filtering error ( $\sigma_{\phi,max}$ —in terms of degrees) as follows,

$$CN_{thr} = -10 \cdot \lg \left[ T_{COR} \cdot \sqrt{1 + \frac{2B}{T_{COR} \Delta F_{PLL}}} - T_{COR} \right] \tag{13}$$

$$B = \left( \frac{2\pi}{360} \right)^2 \cdot \left[ \left( \sigma_{\phi,max} - \frac{\sigma_S}{3} \right)^2 - \sigma_F^2 \right]$$

Next, we can determine an equivalent signal-to-noise ratio at the receiver input under the influence of solar radio emission utilizing the following equation (Kaplan 1996),

$$CN_{eq} = -10 \cdot \lg \left[ 10^{-0.1CN_0} + \frac{10^{0.1JS}}{r \cdot Q \cdot F_{PRN}} \right] \tag{14}$$

where  $CN_0 = 10 \cdot \lg(P_{min})$  is the signal-to-noise ratio in terms of dBW at the receiver input, determined for the minimum power of the received signal,  $Q$  is the parameter of the spectral distribution of the external radio emission relative to the desired signal spectrum ( $Q = 1$  for a narrow-band interference and  $Q = 2$  for a wide-band Gaussian interference),  $JS$  is the relationship between the jamming solar radio emission power and the satellite signal power (dBW), and  $r$  is the coefficient considering distortion of the correlation integral when using “semicodeless” or “codeless” technique for encrypted P(Y) or BT-code signal extracting.

The coefficient  $r$  can be calculated as follows:

$$r = \frac{2\Delta F_{PD}}{F_{PRN}} 10^{0.1(SN_{cor} - \Delta SN_{cor})} \tag{15}$$

Here, the gain in the signal-to-noise ratio due to the correlation processing  $SN_{cor}$  can be determined from Eq. (8), while the value of the correlation processing losses  $\Delta SN_{cor}$  is defined as difference between signal-to-noise ratio of ideal and real correlation receivers. The approximate  $\Delta SN_{cor}$  values were given above for “semi-codeless” and “codeless” correlation techniques (Chen et al. 2005).

It is interesting to know how solar flux irradiation in units of sfu is related to the “ambient noise floor” of the GPS/GLONASS receiver. It would allow us to assess how many “extra sfus” are required to get a certain signal-to-noise ratio decrease with noise figures of the given radio frequency chain. In order to achieve this goal, we need to determine the value of the unjammed signal-to-noise ratio

**Table 4** The characteristics of the navigation receiver performance

Characteristics	Parameter value
Noise bandwidth of the third-order phase lock loop (Kaplan 1996)	$\Delta F_{\text{PLL}} = 18 \text{ Hz}$
Allan deviation oscillator phase noise (Kaplan 1996)	$\sigma_f(\tau) = 10^{-10}$
Maximal line-of-sight jerk dynamics	$dR^3/dt^3 = 0 \text{ m}^3/\text{s}^3$
Predetection integration time (Kaplan 1996)	$T_{\text{COR}} = 20 \text{ ms}$
Front-end passband of GPS receiver (Kaplan 1996)	$\Delta F_{\text{GPS}} = 3 \text{ MHz}$
Front-end passband of GLONASS receiver (for each satellite) (Perov and Kharisov 2005)	$\Delta F_{\text{GLN}} = 0.5 \text{ MHz}$
Correlation losses for “semicodeless” correlation techniques (Chen et al. 2005)	$\Delta \text{SN}_{\text{cor}} = 17 \text{ dB}$
Correlation losses for “codeless” correlation techniques (Chen et al. 2005)	$\Delta \text{SN}_{\text{cor}} = 27 \text{ dB}$
Maximum value of the phase filtering error (Kaplan 1996)	$\sigma_{\phi, \text{max}} = 15^\circ$
Receiver thermal noise power under $T = 290 \text{ K}^\circ$ (Kaplan 1996)	$N = -204 \text{ dBW}$

$CN_0$  in terms of dBW taking into account all the total ambient noise figure sources as follows (Kaplan 1996),

$$CN_0 = P_{\text{min}} + G(\beta) - 10 \cdot \lg(m \cdot T_0) - N_f - L \quad (16)$$

where  $P_{\text{min}}$  is the minimal received signal power in dBW, determined according to the Interface Control Documents of GPS or GLONASS,  $G(\beta)$  is the receiving antenna power gain (Table 1), the term  $10 \cdot \lg(m \cdot T_0)$  is the ambient thermal noise density at the temperature of  $T_0$  (K),  $m = 1.38 \times 10^{-23}$  (W s/K) is the Boltzman’s constant,  $N_f$  is the noise figure of receiver that includes antenna and cable losses in units of dB, and  $L$  denotes the implementation losses, including AD converter loss in dB.

Finally, we can determine the unsafe threshold of solar radio emission power, which could cause GPS and GLONASS navigation satellite signals tracking loss under the given characteristics of the navigation receiver performance. Table 4 presents standard conditions of the GPS and GLONASS receiver performance with estimated threshold signal-to-noise ratio.

The maximum allowable phase filtering error value  $\sigma_{\phi, \text{max}} = 15^\circ$  is determined with Monte Carlo simulation of GPS receiver phase lock loop performance under the combined dynamic and signal-to-noise ratio conditions (Kaplan 1996). Considering the characteristics in Table 4 and using the Eq. (13), we have determined the minimum allowable signal-to-noise ratio at the receiver input,  $CN_{\text{thr}}$  for frequencies L1 and L2 of GPS and GLONASS. In the case under consideration, the  $CN_{\text{thr}}$  values of GPS and GLONASS turned out to be very close to each other: 24.59 and 24.56 dB for L1 and L2, respectively.

The values of unjammed  $CN_0$  ratio were computed with the Eq. (16), taking in account that  $T_0 = 290 \text{ K}$ ,  $N_f = 4 \text{ dB}$ ,  $L = 2 \text{ dB}$  (Kaplan 1996) and  $G(\beta) = -2 \text{ dB}$  ( $\beta > 15^\circ$ , Table 1). Corresponding values of equivalent signal-to-noise ratio at the receiver input,  $CN_{\text{eq}}$  under the direct influence of solar radio emission, are calculated using data of solar radio emission power (Table 3), which are transformed into a jam-to-noise ratio in terms of dBW

( $JS$  in the Eq. 14). Figure 2 presents results of these calculations for L1 and L2 signals of GPS and GLONASS. The horizontal solid lines in all figures show the minimum allowable signal-to-noise ratio at the receiver input  $CN_{\text{thr}}$ , and the horizontal dotted and dash-dotted lines stand for unjammed  $CN_0$  values for CA (CT) code (pink lines), P(Y) or the BT code at frequency L1 (blue lines) and for P(Y) or the BT code at frequency L2 (black lines), respectively. The other curves show the  $CN_{\text{eq}}$  values for the CA (CT) code (pink curves), P(Y) or the BT code at frequency L1 (blue dotted curves) and P(Y) of the BT code at frequency L2 (black dash-dotted curves).

Three cases were considered: (1) the ranging code on the receiving side is well known, and there are no correlation losses (Fig. 2a, b); (2) “semicodeless” (Fig. 2c, d) and (3) “codeless” processing (Fig. 2e, f) for signal extraction with using unknown code.

From Fig. 2, we can conclude that the signal of C/A (CT) code at L1 frequency turned out to be the most resistant to the influence of the solar radio emission. The equivalent signal-to-noise ratio for the CT signal (GLONASS) in the case under consideration is higher than the  $CN_{\text{thr}}$  critical level, even under the influence of the solar radio emission flux of  $10^6$  sfu (Fig. 2a, b). At the same time, the  $CN_{\text{eq}}$  value for the C/A signal (GPS) reduces more noticeably and can drop below  $CN_{\text{thr}}$  level when solar radio noise power is just about  $10^6$  sfu (Fig. 2a). Thus, we can expect the failure in the C/A signal tracking when the power level of solar radio noises is  $\approx 10^6$  sfu. In our opinion, this conclusion can be explained with the idea that the front-end passband of the GPS receiver radio chain is wider than that one of GLONASS receiver particular satellite radio channels. Hence, integral power of the solar radio noise which penetrates into a GPS receiver is higher in comparison with the GLONASS one.

When high-precision ranging codes (P(Y) and BT) on the receiving side are known, stable tracking of these signal components in GPS and GLONASS receivers is provided with a high quality even under the influence of solar radio

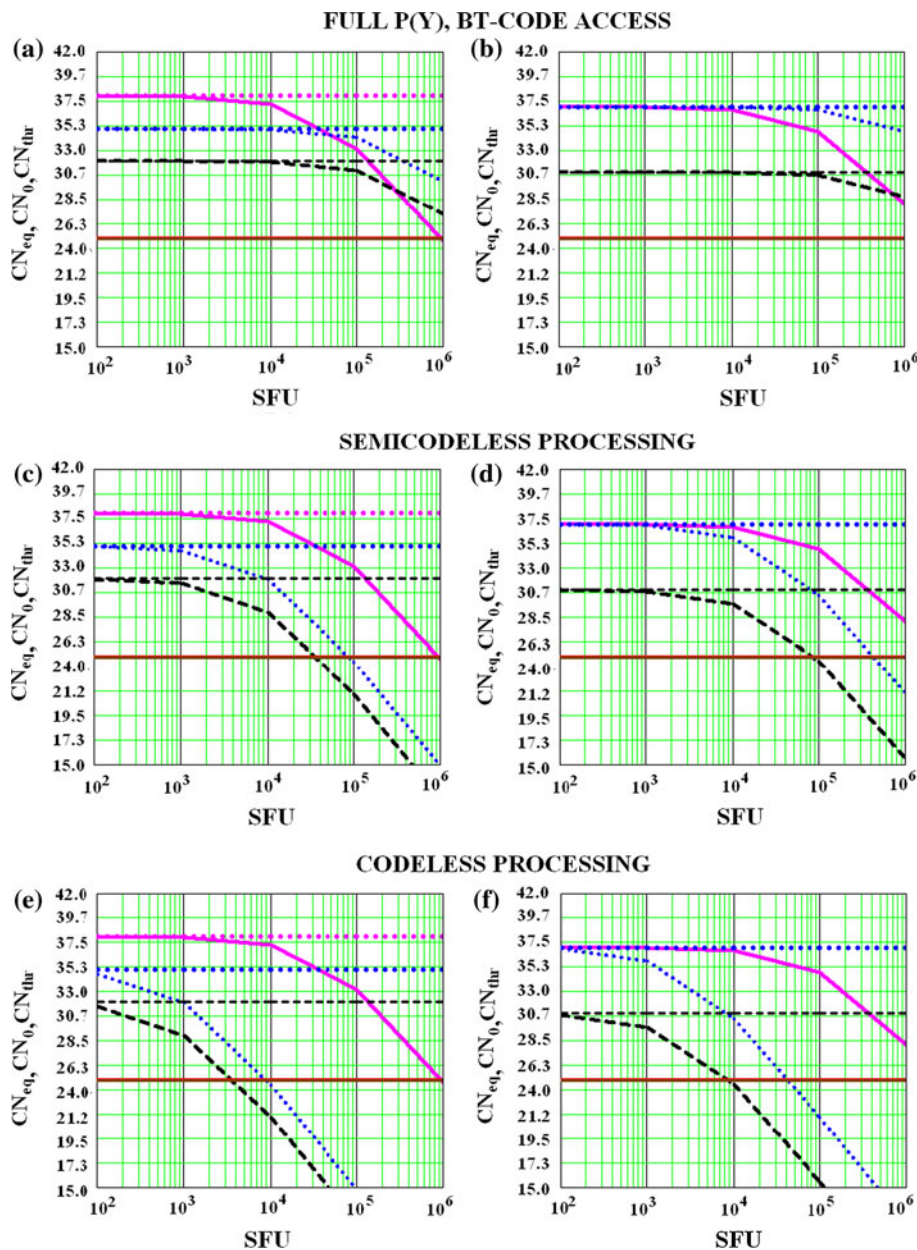
noises of more than  $10^6$  sfu (Fig. 2a, b). However, signal tracking of these components can fail when the power level of solar radio emission is more than 38,000 sfu (the P(Y) component at frequency L2, Fig. 2c) when the “semi-codeless” correlation processing is used. Since the power of P(Y) and BT signal components at frequency L1 is considerably higher, the tracking of these components may fail when the rate of the solar radio emission flux is more than 100,000 sfu (Fig. 2c, d).

The situation is the worst when the “codeless” processing of encrypted signals is utilized (Fig. 2e, f). One can see that the P(Y) signal tracking fails when the solar radio noise powers are about 4,000 and 10,000 sfu at frequencies L2 and L1, respectively. The corresponding power levels

of the solar radio emission flux that can cause the failure of the BT (GLONASS) signal tracking at frequencies L1 and L2 are 10,000 and 13,500 SFU, respectively.

Note that these estimations have been obtained for relatively favorable initial conditions, assuming relatively good Allan deviation factor and no dynamic stress or vibrations. We have also ignored effects of amplitude and phase ionospheric scintillations, which may cause significant fading of signal amplitude at the receiver antenna output. The multipath-propagation effect of signals in the reception point has also been ignored. Nevertheless, we have obviously proven the negative effect of powerful solar radio emission on the GPS and GLONASS performance.

**Fig. 2** An equivalent signal-to-noise ratio at GPS (GLONASS) navigation receiver input under direct influence of the solar radio emission in units of sfu



### Experimental statistics of GPS phase slips and counts omission during powerful solar flares

We use GLOBDET software developed at the ISTEP SB RAS to process GPS data from the global network of dual-frequency receivers (Afraimovich 2000). Our database of GPS RINEX (Receiver Independent Exchange Format) files consists of data from over 1,500 GPS sites (<http://sopac.ucsd.edu/other/services.html>). For December 6, 2006, we used RINEX files from the CORS network (262 sites at <ftp://www.ngs.noaa.gov/cors/rinex/>). We also employ data from the Japanese GPS network GEONET (about 1,225 stations) for December 13, 2006.

Figure 3 shows the experimental geometry of GPS measurements during the solar flare on December 6 and 13, 2006. The GPS sites are marked by dots. The names of the sites are not given due to the space limitation. Stars indicate the location of sunlit points for the solar flare on December 6 and 13, 2006.

We calculate the 30 s series of the L1–L2 phase difference on two GPS frequencies  $f_1$  and  $f_2$  along lines of sight (LOS) of “receiver-satellite” to confirm a slip in measurements of the L1–L2 phase difference (Afraimovich et al. 2002a). These data for each GPS satellite are then averaged over a period of  $dT = 5$  min at all chosen sites. It allows us to calculate the average observation density  $M(t)$  and slip density  $S(t)$  for all  $n$  LOS. Further, we calculate the average relative density of slips  $P(t) = S(t)/M(t)$  by percentage and determine the maximal value  $P_{\max}$  by percentage. If the next count in a RINEX file is absent, the number of slips is equated to that of expected observations, so the density of slips becomes equal to 100%.

Failures in L1–L2 make precision positioning in the dual-frequency mode impossible. The positioning is generally impossible if the signal at both GPS operating frequencies is not received at all. In order to estimate a probability of such failures for all LOS, we define a number of counts omission  $N(t)$  for each 30-s observation epoch. Considering  $M(t)$  as an expected observation density within

the current 30-s epoch, we define counts omission density as  $W(t) = N(t)/M(t)$ . We also determine the corresponding maximum value  $W_{\max}$ . The 30-s time resolution of the  $W(t)$  rows allows us to conduct a detailed analysis of time behavior of  $W(t)$  values under the solar radio emission flux variations.

In order to compare GPS and GLONASS noise immunity, we compute the relative slip density  $Q(t)$  in percent of the main signal parameters: L1, L2 (signal carrier phase), and C1, P1, P2 (C/A (CT) and P(Y)(BT) code delay) at  $f_1$  and  $f_2$  GPS and GLONASS frequencies. A measurement slip we considered as an event when the current 30-s count of corresponding GPS parameters equals to zero or this count was absent in the RINEX file.

Unfortunately, there were much fewer combined GPS/GLONASS data set since there were only 44 combined GPS/GLONASS sites available. Using these data, we were able to investigate GPS measurement slips in more details. We utilized the combined GPS/GLONASS data set to conduct the comparative analysis of GPS and GLONASS noise immunity under the direct solar radio emission interference.

The combined GPS/GLONASS data set was processed with a particular method. The essence of this method is to compute the sum of L1, L2, P1, P2 and C1 measurement slips separately for each parameter of GPS and GLONASS. This calculation is conducted for each current 30-s observation epoch for all GPS/GLONASS sites. The event when every of L1, L2, P1, P2 or C1 values is absent or equals to zero is considered as a measurement slip of this parameter. Whenever L1, L2, P1, P2 and C1 measurements are absent simultaneously at the same observation epoch, we suppose this event has also a measurement slip. An averaged slip density  $Q(t)$  value was computed next for each of these parameters at the each 30-s epoch.

The data set of 44 GPS/GLONASS sites relating to solar radio bursts on December 6 and 13, 2006, was processed. Due to uneven distribution of GPS/GLONASS sites on the earth surface, there were only 4 and 7 sites available within the sunlit side of the earth on December 6 and 13, respectively.

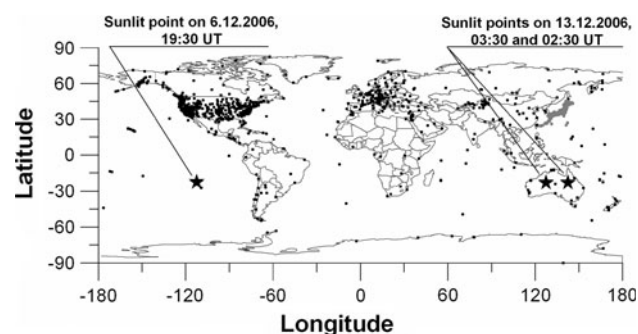


**Fig. 3** GPS measurement geometry during the solar flares on December 6 and 13, 2006. The GPS sites are marked by dots. Asterisks show the location of sunlit points for the solar flares

### GPS phase slips and counts omission as a result of solar radio bursts on December 6, 2006

According to the data from the Owens Valley Solar Array (OVSA), the power of solar radio emission on December 6, 2006, in the GPS frequency band exceeded  $10^6$  sfu. The background emission level is about  $\sim 10$ – $10^2$  sfu. Figure 4e shows the RHCP radio emission spectrum at 1.2–2.0 GHz, registered at the Solar Radio Spectrograph OVSA. The planetary index of geomagnetic activity was  $K_p \sim 4$ .

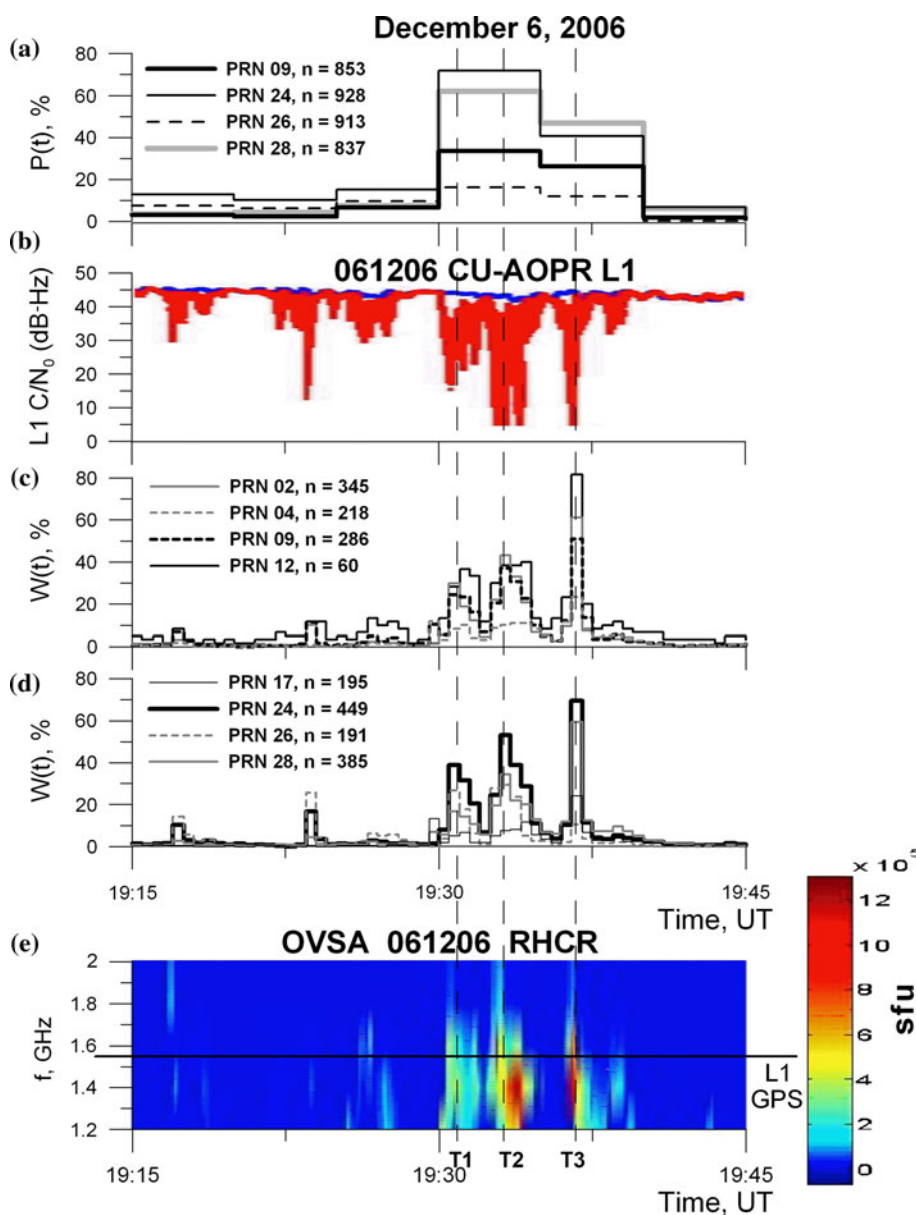
Figure 4a presents the  $P(t)$  time dependences on the earth sunlit side ( $200\text{--}300^\circ\text{ E}$ ;  $-80 + 80^\circ\text{ N}$ ). These  $P(t)$  data were derived from  $n = 12,793$  LOS observations for all observable GPS satellites which were recognized with their pseudo random noise (PRN) code numbers at the elevation angles  $\Theta > 10^\circ$  during the observation time from 18:00 to 20:00 UT (heavy black line). Figure 4a shows significant increasing of the  $P(t)$  within 19:30–19:40 UT above the background level of slips, which usually does not exceed  $P_{\max} \sim 0.2\text{--}0.3\%$  for such weakly disturbed ionosphere (Afraimovich et al. 2002b). Sharp increasing of  $P(t)$  values corresponded to an abrupt increasing of the solar radio emission flux at the very period of time.

The maximum relative density value of slips  $P_{\max} = 68.5\%$  exceeded the background one in about  $\sim 50$  cases.

At the same time, the average density  $P(t)$  on the earth night side for  $\Theta > 10^\circ$  and  $n = 3,521$  LOS did not exceed the background one. Unfortunately, the time resolution of  $P(t)$  dependence,  $dT = 5$  min appeared to be insufficient to display the fine time structures of the radio emission flux (Fig. 4e), obtained with the resolution lower than 1 s.

Nevertheless, the concurrence in the form of envelopes of the phase slip distribution and solar radio flux is obvious. One can see that the  $W(t)$  values were observed from 19:15 to 19:45 UT for several PRN satellite numbers (Fig. 4c). It is evident that maximum values  $W_{\max}$  can reach 82 and 69% (PRN12,  $n = 50$  GPS sites; and PRN24,  $n = 299$  GPS sites). It can be seen from Fig. 4b that the sharp increase in phase slips and number of counts omission is totally consistent with the moments of the most powerful

**Fig. 4** GPS L1–L2 phase slips on December 6, 2006



solar radio bursts (moments T1, T2, T3). Deep fading of the signal-to noise ratio at the L1 GPS frequency was observed during the same periods of time. It proves the idea that such sharp fading of GPS signal-to-noise ratio is caused by direct interference of solar radio emission in the 1–2 GHz frequency band.

### GPS phase slips and counts omission as a result of solar radio bursts on December 13, 2006

According to the data from the Learmonth Solar Radio Spectrographs, the total flux  $F(t)$  of radio emission on December 13, 2006, exceeded  $10^5$  sfu at 1,415 MHz (Fig. 5e). Sharp increasing of the solar radio flux power can be noted within the time periods 02:20–02:28 UT (A) and 03:30–03:37 UT (B). The horizontal line marks the spectrograph amplitude saturation level of about  $\sim 110,000$  sfu.

According to the data from the Nobeyama Radio Polarimeters ([http://solar.nro.nao.ac.jp/norp/html/event/20061213\\_0247/norp20061213\\_0247.html](http://solar.nro.nao.ac.jp/norp/html/event/20061213_0247/norp20061213_0247.html)), the RHCP solar radio emission power exceeded  $1.47 \times 10^5$  sfu at 1 GHz at 02:28:09 UT and  $2.57 \times 10^5$  sfu at 2 GHz at 03:35:51 UT on December 13, 2006 (Fig. 5e, the thick gray line and the black line, respectively).

For the December 13 flare on the earth sunlit side ( $40^\circ$ – $200^\circ$  E;  $-80^\circ$  +  $80^\circ$  N), Fig. 5c, d presents  $W(t)$  values of counts omission which were registered for all satellites observed from 02:15 to 03:45 UT. Obviously, the maximum values  $W_{\max}$  can reach 50% and 39% (PRN28,  $n = 16$  GPS sites; and PRN08,  $n = 23$  GPS sites). It has been shown that the sharp increase in slips and count omissions completely coincide with the impulse solar radio bursts during A and B periods, including the fine time structure of solar radio burst.

Since there were too few GPS sites on the earth sunlit side ( $40$ – $200$  E;  $-80$  +  $80$  N) on December 13, 2006 (<http://sopac.ucsd.edu/other/services.html>), we used the data set from the Japanese network GEONET that comprises 1,225 GPS permanent sites. Figure 5a, b shows the dependences  $P(t)$  for the December 13, 2006, flare over Japan for some satellites which were observed from 02:15 to 03:45 UT. Maximum values  $W_{\max}$  can run to 50% (PRN13) and 27% (PRN16). The sharp increase in count omissions coincide with the impulses of solar radio emission during the time intervals A and B.

### GPS phase slips and counts omission as a result of solar radio bursts on October 28, 2003

It is especially interesting to assess GPS measurement slips density caused by the weaker solar radio burst on October 28,

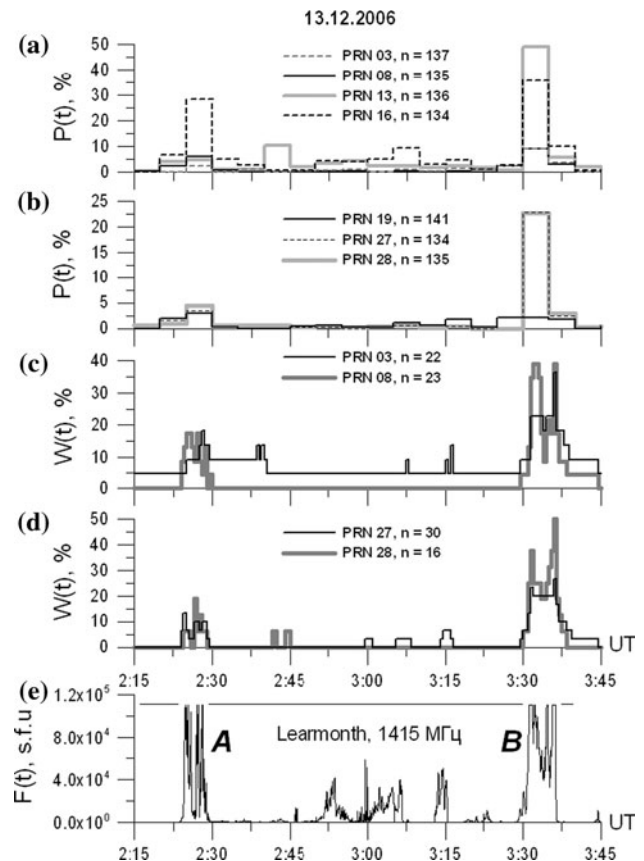


**Fig. 5** GPS L1–L2 phase slips on December 13, 2006

2003. The power of this burst was by 3 orders of magnitude less than the solar radio bursts on December 6 and 13, 2006.

According to the data from the Trieste Solar Radio Spectrograph, Italy, the RHCP solar radio noise level exceeded  $3 \times 10^3$  sfu at 1,420 MHz on October 28, 2003 (Fig. 6e). There are two solar radio bursts when the power of radio emission flux exceeded the level of  $3 \times 10^3$  sfu: within the time periods from 11:05 to 11:08 UT (time interval A) and from 11:40 to 12:00 UT (time interval B).

Figure 6d (black line) presents  $P(t)$  dependences for the October 28, 2003, flare on the earth sunlit side ( $330$ – $120^\circ$  E;  $-80$  +  $80^\circ$  N) derived from  $n = 2,452$  LOS observations, for all observable satellites at the elevation angle  $\Theta > 10^\circ$  during the time period from 11:00 to 12:00 UT. A significant excess of the background level,  $P_{\max} \sim 0.2$ – $0.5\%$ , was observed from 11:02 to 11:10 UT. This event corresponds to an abrupt increase in the solar radio emission flux during time interval A. The maximum value  $P_{\max} = 1.7\%$  exceeds the background one in about  $\sim 3$ – $4$  times. At the same time, the average density of slips on the night side of the earth for  $\Theta > 10^\circ$  ( $n = 12,070$  LOS) does not exceed the background one (Fig. 6d, thin gray line).

More substantial evidence on GPS functioning quality deterioration can be found by estimating the average

relative density of slips for separate GPS satellites. In Fig. 6a–c, the  $P(t)$  dependences are given for some satellites observed during the time period 10:00–12:00 UT. The maximum values  $P_{\max}$  can reach 11 and 10.2% (for PRN05 and PRN18,  $n = 100$ ), whereas the value  $P_{\max} = 2.3\%$  for satellite PRN29 is close to  $P_{\max} = 1.7\%$ , which was determined for all satellites. The sharp increasing of slips density and count omissions happened simultaneously with the most powerful solar radio bursts for the time intervals A and B. Though power of the solar radio burst on October 28, 2003, is by 2–3 orders of magnitude less than that on December 6 and 13, 2006, the maximum values of phase slips are smaller by only in 5–10 times. Unfortunately, the combined GPS/GLONASS data set was not enough in order to analyze the solar radio burst effect on October 28, 2003.

### Comparative analysis of GPS and GLONASS performance

It is known that the basic principles of GLONASS and GPS functioning are almost identical from the viewpoint of

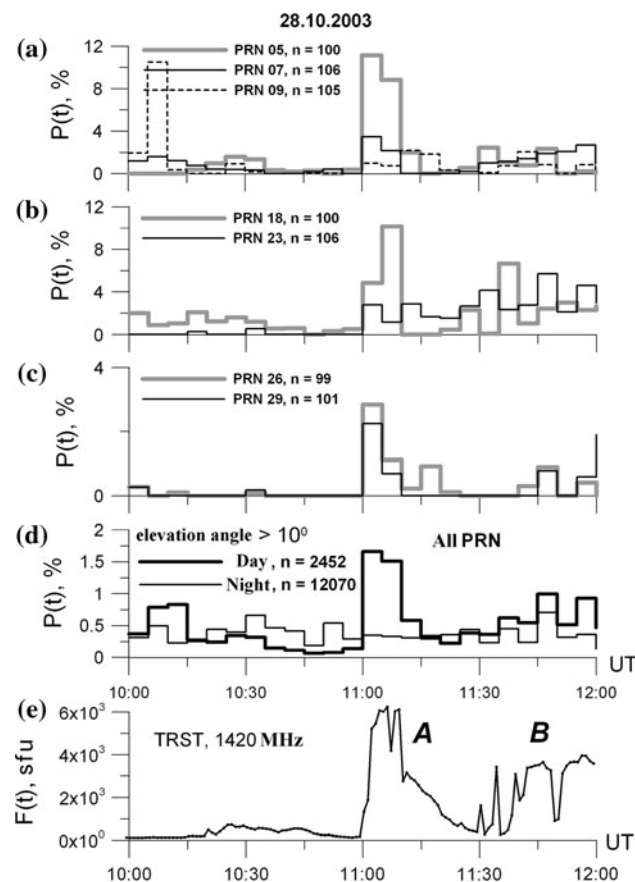


**Fig. 6** GPS L1–L2 phase slips on October 28, 2003

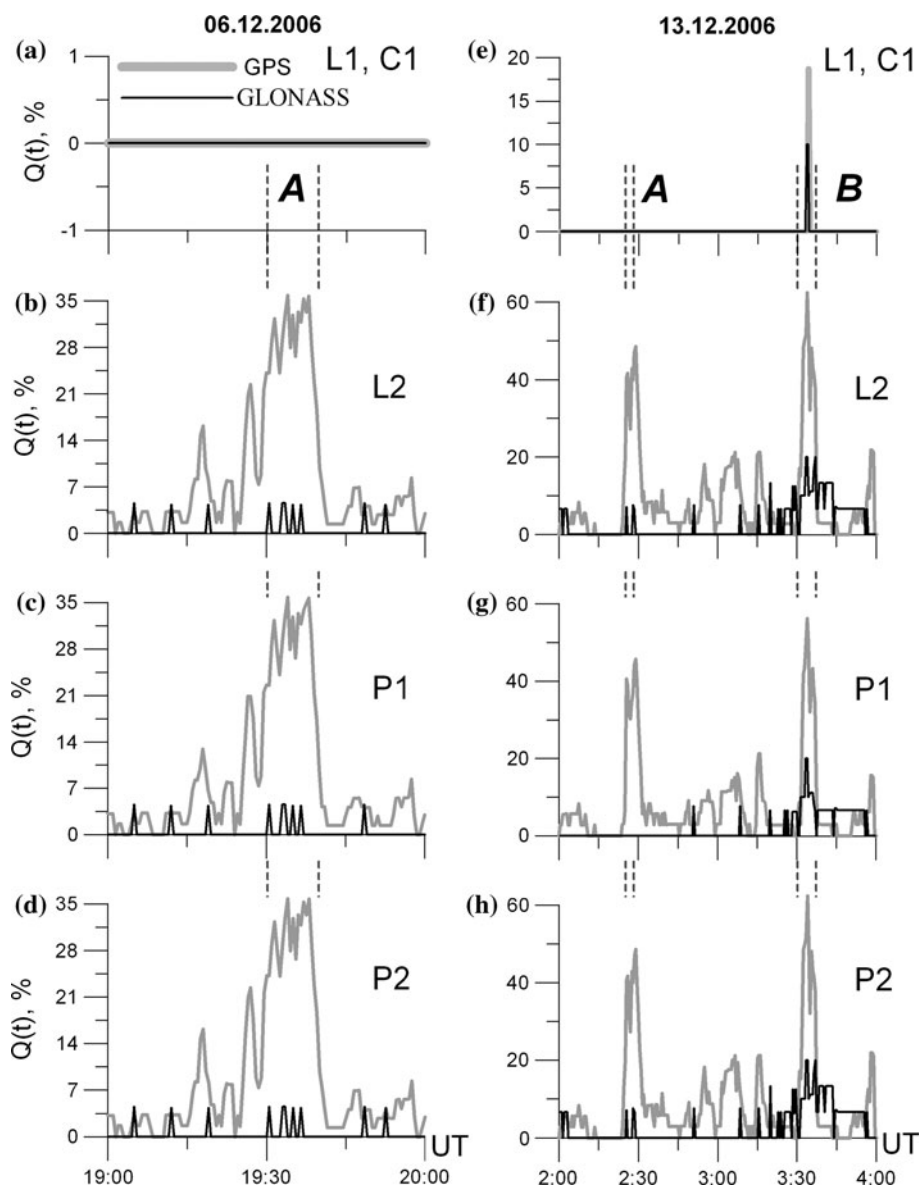
estimation of the signal power. Hence, a comparative analysis of the GPS and GLONASS receiver noise immunity under direct interference of the solar radio emission is of obvious interest. For example, in the case of GLONASS, the normalized minimum power should not be less than  $-157$  dBW at the main operating frequency of GLONASS (1,600 MHz) and  $-163$  dBW at the auxiliary frequency 1,250 MHz (ICD-GLONASS 2002). The corresponding standard for GPS determines these values as  $-163$  dBW at the main frequency of GPS (1,545.42 MHz) and  $-166$  dBW at the second operating frequency (1,227.6 MHz) (ICD-GPS-200c 1993). As we can conclude from the Fig. 1, signal-to-noise ratio at GLONASS receiver antenna output is 7 dB lower than the GPS one under the same solar radio emission power. It seems that we should expect lower noise immunity for GLONASS receivers under the same level of solar radio emission interference. However, it turned out that GPS receivers presented lower noise immunity under solar radio bursts interference on December 6 and 13, 2006.

Figure 7 presents relative densities  $Q(t)$  of L1, C1, L2, P1 and P2 measurement failures, respectively, which were computed for all observed GPS satellites (thick gray curves) and GLONASS satellites (thin black curves) registered within the sunlit zone on December 6 and 13, 2006. Symbols A (December 6) and B (December 13) mark the time intervals when the maximal level of solar radio emission power was  $>10^6$  sfu (December 6) and  $>10^5$  sfu (December 13), respectively. As one can see, there is high reliability of L1 and C1 measurements on the main operating frequency of both GPS and GLONASS systems even in the periods “A” and “B” (Fig. 7a, e). No failures of L1 and C1 parameter were detected on December 6 (Fig. 7a). Only coincident short failures of L1 and C1 measurements were found simultaneously for both GPS and GLONASS at 03:34 UT (Fig. 7e). The results are in good agreement with the idea that if we know the ranging code structure exactly, we do not have correlation losses and the unsafe level of solar radio emission is about  $10^6$  sfu for both GPS and GLONASS.

The situation is the worst when we utilize the codeless method in order to extract the P(Y) or BT code, in which case we have correlation losses is about 27 dB. We can see sharply increasing  $Q(t)$  values by up to 35% on December 6, 2006, in P1, P2 and L2 parameters of GPS in the very period of sharply increasing solar radio emission power (Fig. 7b, c, d). The situation turned out to be more dramatic on December 13, 2006. One can see the value  $Q(t)$  of P1, P2 and L2 parameters exceeds 50% within periods “A” and “B” (Fig. 7f, g, h).

More important result consists of the fact that the maximum  $Q(t)$  value of all signal parameters of GLONASS, excepting for L1 and C1, is lower than the one for

**Fig. 7** A comparative analysis of GPS and GLONASS noise immunity under powerful solar radio emission interference on December 6 and 13, 2006



GPS by a factor of 2–4. In our opinion, this advantage is due to the fact that a GLONASS receiver can perform its function more reliably under conditions of the powerful solar radio interference because of the narrower front-end passband of the GLONASS receiver for the separate GLONASS satellites compared to the GPS receivers. Unfortunately, the small statistics did not allow us to get more statistically significant assessments. We will further investigate it in details.

As the whole, results in Fig. 7 prove our theoretical assessments of the unsafe level of solar radio emission when GPS (GLONASS) signal tracking failures appear. The comparison between global failures of the GPS and GLONASS shows that the unsafe level of solar radio emission for GLONASS is higher than GPS.

## Conclusion

This research the solar radio noise power at the GPS and GLONASS receiver antenna output when the power level of the solar radio emission flux is known. Theoretical examination of L1 and L2 GPS/GLONASS signal tracking reliability under the direct influence of the powerful solar radio emission in L-band has been conducted under the main assumption for both GPS and GLONASS with the same effective antenna area, the same correlation losses of encrypted BT and P(Y) signal tracking and the same tracking loop parameters (Table 4). We have obtained the “unsafe” power level of the solar radio emission that could cause failures of GPS and GLONASS signal tracking. It was found that signal tracking started to fail when the solar

radio emission power is about 4,000 sfu at the GPS frequency L2 and 10,000 sfu at the frequency L1 when the “codeless” correlation processing technique is utilized. These assessments for GLONASS turned out to be 10,000 and 13,500 sfu at frequencies L1 and L2, respectively. Hence, the GLONASS navigation receivers are more resistant to intensive solar radio emission under considered conditions. In our opinion, this occurs because the GLONASS receiver radio chain is characterized with a narrower front-end passband in order to provide effective extraction of signals of the particular GLONASS satellites.

Our theoretical assessments are proven by experimental statistics of GPS phase slips and counts omission that was found during powerful solar flares condition on December 6 and 13, 2006, and especially, during the much weaker solar radio burst condition on October 28, 2003. It is very important to emphasize that although power of the solar radio burst on October 28, 2003, is by 2–3 orders of magnitude less than that on December 6 and 13, 2006, the maximum values of phase slips are only 5–10 times less. Particular slips of L1–L2 phase measurements started to appear under the interference of solar radio flux when power was just a bit higher than  $10^3$  sfu.

Experimental results have shown that for over 10–15 min, the high-precision GPS positioning was partially disrupted on sunlit sides of the earth on December 6 and 13, 2006. The high level of phase slips and count omissions resulted from the wideband solar radio noise emission. The statistics of phase slips obtained in this study for sunlit sides of the earth confirms the suppression effect of GPS receiver performance during the December 6, 2006, flare with more reliability than the previously published, which were obtained and discussed at only several GPS sites by Carrano et al. (2007) and Cerruti et al. (2006).

In general, our results are in good agreement with earlier results by other authors, which indicate that direct impact of the solar radio emission can cause failure in GPS signal tracking of navigation receivers, even if the solar radio emission power is relatively low (about  $10^3$  sfu). It proves that solar radio noises of more than  $10^3$  sfu can have a negative influence on the GPS/GLONASS performance.

**Acknowledgments** Authors express profound gratitude to Prof. G. Ya. Smolkov for his support and interest in this investigation, Dr. V. V. Grechnev for his help in using the 1 and 2 GHz data of the Nobeyama Radio Polarimeters and colleagues from the Nobeyama Radio Observatory, for solar radio emission data on December 13, 2006, as well as the IGS (<http://lox.ucsd.edu/cgi-bin/al-1Coords.cgi?>) and GEONET ([ftp://terras.gsi.go.jp/data/GPS\\_products/](ftp://terras.gsi.go.jp/data/GPS_products/)) for RINEX data. The work is supported by the Siberian Branch of the Russian Academy of Sciences and the Program of basic research of the Presidium of the Russian Academy of Sciences “Solar activity and physical processes in the Sun–Earth system”. Finally, the authors wish to thank the referees for their valuable suggestions which allowed us to improve the quality of the manuscript.

## References

- Afraimovich EL (2000) GPS global detection of the ionospheric response to solar flares. *Radio Sci* 35(6):1417–1424
- Afraimovich EL, Lesyuta OS, Ushakov II, Voeykov SV (2002a) Geomagnetic storms and the occurrence of phase slips in the reception of GPS signals. *Ann Geophys* 45(1):55–71
- Afraimovich EL, Zhrebtsov GA, Smolkov GYa (2002b) Total failure of GPS during a solar flare on December 6, 2006. *Rep Earth Sci* 417(8):1231–1235
- Afraimovich EL, Demyanov VV, Ishin AB, Smolkov GYa (2008) Powerful solar radio bursts as a global and free tool for testing satellite broadband radio systems, including GPS–GLONASS–GALILEO. *J Atmos Sol Terr Phys* 70:1985–1994
- Carrano CS, Groves KM, Bridgwood CT (2007) Effects of the December 2006 solar radio bursts on the GPS receivers of the AFRL–SCINDA network. In: Doherty PH (ed) *Proceedings of the international beacon satellite symposium*, June 11–15
- Cerruti AP, Kintner PM, Gary DE, Lanzerotti LJ, de Paula ER, Vo HB (2006) Observed solar radio burst effects on GPS/WAAS carrier-to-noise ration. *Space Weather* 4:S10006. doi: [10.1029/2006SW000254](https://doi.org/10.1029/2006SW000254)
- Chen Z, Gao Y, Liu Z (2005) Evaluation of solar radio bursts’ effect on GPS receiver signal tracking within international GPS service network. *Radio Sci* 40:RS3012. doi: [10.1029/2004RS003066](https://doi.org/10.1029/2004RS003066)
- ICD–GPS–200c (1993) Interface control document. <http://www.navcen.uscg.gov/pubs/gps/icd200/ICD200Cw1234.pdf>
- ICD–GLONASS (2002) Interface control document (in Russian). [http://www.glonassgsm.ru/upl\\_instructions/-ICD-2002r.pdf](http://www.glonassgsm.ru/upl_instructions/-ICD-2002r.pdf)
- Jin SG, Luo O, Park P (2008) GPS observations of the ionospheric F2-layer behavior during the 20th November 2003 geomagnetic storm over South Korea. *J Geod* 82(12):883–892. doi: [10.1007/s00190-008-0217-x](https://doi.org/10.1007/s00190-008-0217-x)
- Kaplan ED (ed) (1996) *Understanding GPS: principles and applications*. Artech House, Norwood
- Klobuchar JA, Kunches JM, Van Dierendonck AJ (1999) Eye on the ionosphere: potential solar radio burst effects on GPS signal to noise. *GPS Sol* 3(2):69–71
- Perov AI, Kharisov VN (ed) (2005) *GLONASS. Structure and principles of functioning* (in Russian), Edition of Radioelectronics. Moscow
- Skone S, de Jong M (2001) Limitations in GPS receiver tracking performance under ionospheric scintillation. *Phys Chem Earth A* 26(6–8):613–621

## Author Biographies

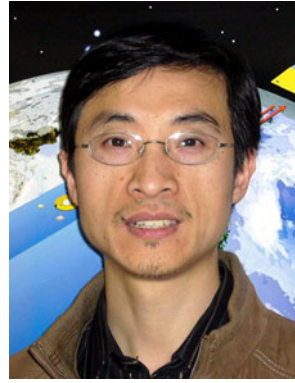


**Vladislav Demyanov** got his Doctor of Science degree in 2011 from Siberian Federal University under Prof. Afraimovich E. L. supervision. Now he works as an associate professor at Irkutsk State Railway University. The main field of his scientific interests is GPS/GLONASS performance under geo-space disturbed condition. He is an author of more than 50 research papers, 5 inventions and scientific mentor of 4 PhD students.



**Edward Afraimovich** (March 12, 1940—November 8, 2009) founded the Irkutsk school of ionosphere GPS sounding in 1998. His main scientific interests were connected with experimental research on ionospheric fine structure, based on processing data from the global GPS network. Most of his life he worked in the Institute of Solar-Terrestrial Physics SB RAS (Irkutsk, Russia). Twenty-four PhD students graduated under his supervision. He published more than 200 papers in reviewed journals and 2 monographs and received 10 invention certificates.

published more than 200 papers in reviewed journals and 2 monographs and received 10 invention certificates.



Book GNSS (2011).

**Shuanggen Jin** is a Professor & Group Head at Shanghai Astronomical Observatory, CAS. He has focused on GNSS Navigation & Reflectometry, Remote Sensing & Climate Change, and Space/Planetary Sensing & Dynamics and published over 70 peer-reviewed journal papers in JGR, GJI, IEEE, J. Geodesy, etc. and 10 books/chapters. He has been President of the IAG Sub-Commission 2.6 (2011–2015), Editor-in-Chief of Int. J. Geosci. (2010) and Editor of